Supporting Information For

Pyridyl-Directed C-H and C-Br Bond Activations Promoted by Dimer Iridium-Olefin Complexes

Pierre-Luc T. Boudreault,[†] *Miguel A. Esteruelas,**[‡] *Erik Mora,*[‡] *Enrique Oñate,*[‡] *and Jui-Yi Tsai*[†]

[‡]Departamento de Química Inorgánica, Instituto de Síntesis Química y Catálisis Homogénea (ISQCH), Centro de Innovación en Química Avanzada (ORFEO-CINQA), Universidad de Zaragoza-CSIC, 50009 Zaragoza, Spain

[†]Universal Display Corporation, 375 Phillips Boulevard, Ewing, New Jersey 08618, United States

*Corresponding author's e-mail address: maester@unizar.es

CONTENTS

Instrumental methods. Solvents were dried using standard procedures and distilled under argon atmosphere or obtained dry from an MBraun solvent purification apparatus. NMR spectra were recorded on either a Bruker Avance 300 MHz or 400 MHz instrument. Signals were assigned using also bidimensional NMR experiments (^{1}H-^{1}H COSY, ^{1}H-^{13}C{^{1}H} HMBC and ^{1}H-^{13}C{^{1}H} HSQC). Elemental analyses were carried out using a Perkin-Elmer 2400 CHNS/O analyzer, and IR spectra were measured using a PerkinElmer Spectrum 100 FT-IR spectrometer, equipped with an ATR accessory, as pure solids. High-resolution electrospray mass spectra were acquired using a MicroTOF-Q hybrid quadrupole time-of-flight spectrometer (Bruker Daltonics, Bremen, Germany). MALDI-TOF mass spectra were acquired using a Bruker Autoflex III, MALDI-TOF/TOF equipped with a DCTB matrix.

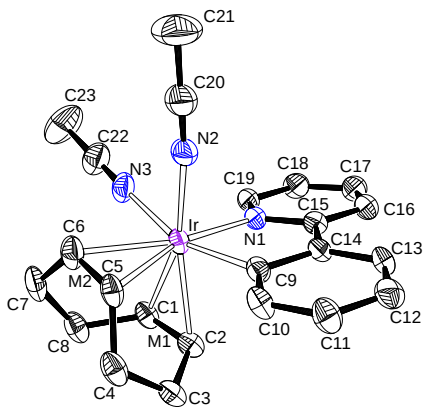

Figure S1. ORTEP diagram of complex **11** (50% probability ellipsoids). Hydrogen atoms are omitted for clarity. Selected bond lengths (Å) and angles (deg): Ir-N(1) = 2.077(4), Ir-N(2) = 2.044(5), Ir-N(3) = 2.132(6), Ir-C(9) = 2.078(6), Ir-C(1) = 2.195(6), Ir-C(2) = 2.215(6), Ir-C(5) = 2.256(6), Ir-C(6) = 2.265(6), N(3)-Ir-C(9) = 160.7(2), N(2)-Ir-M(1) = 175.5(2), N(1)-Ir-M(2) = 176.8(2).

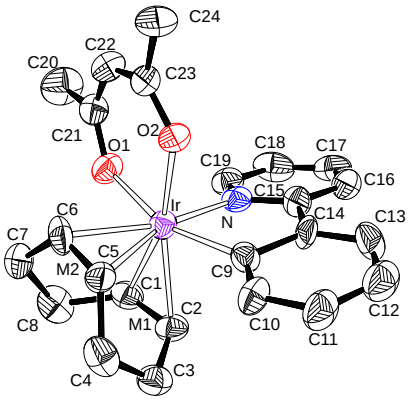

Figure S2. 12 crystallizes with two chemically equivalent molecules in the asymmetric unit. ORTEP of complex **12** (50% probability ellipsoids). Hydrogen atoms are omitted for clarity. Selected bond lengths (Å) and angles (deg): Ir-N = 2.082(10), 2.059(11), Ir-O(2) = 2.068(8), 2.062(9), Ir-O(1) = 2.139(9), 2.137(9), Ir-C(9) = 2.068(13), 2.077(13), Ir-C(1) = 2.185(13), 2.171(13), Ir-C(2) = 2.218(13), 2.210(12), Ir-C(5) = 2.236(13), 2.240(14), Ir-C(6) = 2.193(13), 2.205(13), O(1)- Ir-C(9) = 160.0(4), 159.9(4), O(2)- Ir-M(1) = 174.7(5), 174.3(5), N-Ir-M(2) = 177.3(5), 177.1(5).

Structural Analysis of Complexes 5, 6, 9, 10, 11 and 12. X-ray data were collected for the complexes on a Bruker Smart APEX and Bruker Smart APEX DUO diffractometer equipped with a normal focus, and 2.4 kW sealed tube source (Mo radiation, l = 0.71073 Å). Data were collected over the complete sphere covering 0.3° in w. Data were corrected for absorption by using a multiscan method applied with the SADABS program.[1] The structures were solved by Patterson or direct methods and refined by full-matrix least squares on F^2 with SHELXL2016,[2] including isotropic and subsequently anisotropic displacement parameters. The hydrogen atoms were observed in the least Fourier Maps or calculated, and refined freely or using a restricted riding model. The disordered molecules were refined with different moieties, restrained geometries, and complementary occupancy factors.

Complex **5** has two bromophenyl-pyridine (C_6H_3Br-py) and an acac ligands so the molecule has a symmetry axis C2 over the iridium atom and crystallizes in the monoclinic C2/c space system (Z'=0.5). Complex **6** has a very similar structure with one bromophenyl-pyridine (C_6H_4-py), one pyridine (C_6H_3Br-py) and one acac ligands. This molecule lacks any kind of symmetry but crystallizes in a unit cell similar to **5** with two possible space groups C2/c (Z'=0.5) or Cc (Z'=1). Two alternative refinements were performed. One with the symmetric C2/c space system with occupancy 0.5 in the bromine position, and other in the asymmetric Cc space group with the bromine atoms in two positions with final occupancies 0.88/0.12. The refinement in the asymmetric space group was more consistent and then selected (agreement factors, positive and negative residuals...).

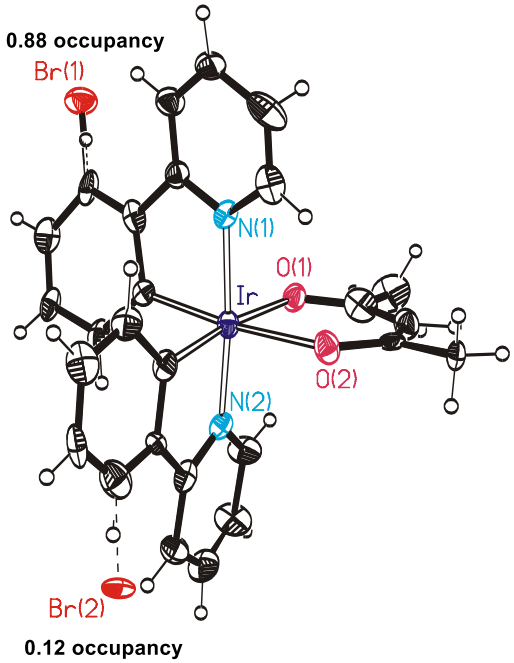

Figure S3. ORTEP of complex **6**.

Crystal data for **5**: $C_{27}H_{21}Br_2IrN_2O_2$, M_W 757.48, yellow, irregular block (0.252 x 0.024 x 0.023 mm^3), monoclinic, space group C2/c, *a*: 12.506(2) Å, *b*: 26.238(5) Å, *c*: 7.2648(13) Å, *β*: 100.937(2)°, V = 2340.4(7) $Å^3$, Z = 4, Z' = 0.5, D_{calc}: 2.150 g cm^{-3},

F(000): 1440, T = 100(2) K, m 9.148 mm^{-1}. 10195 measured reflections (2θ: 3-57°, w scans 0.3°), 2797 unique (R_{int} = 0.0743); min./max. transm. Factors 0.627/0.862. Final agreement factors were R^1 = 0.0517 (2236 observed reflections, I > 2s(I)) and wR^2 = 0.1220; data/restraints/parameters 2797/0/156; GoF = 1.091. Largest peak and hole 1.728 (close to iridium atoms) and -2.165 e/ $Å^3$.

Crystal data for **6**: $C_{27}H_{22}BrIrN_2O_2$, M_W 678.57, yellow, irregular block (0.289 x 0.055 x 0.048 mm^3), monoclinic, space group Cc, *a*: 12.050(2) Å, *b*: 26.622(5) Å, *c*: 7.2732(12) Å, *β*: 103.606(2)°, *V* = 2267.8(7) $Å^3$, *Z* = 4, *Z'* = 1, D_{calc}: 1.987 g cm^{-3}, F(000): 1304, T = 100(2) K, m 7.678 mm^{-1}. 19588 measured reflections (2θ: 3-57°, w scans 0.3°), 4848 unique (R_{int} = 0.0414); min./max. transm. Factors 0.546/0.862. Final agreement factors were R^1 = 0.0375 (4302 observed reflections, I > 2s(I)) and wR^2 = 0.0965; data/restraints/parameters 4848/3/310; GoF = 1.042. Largest peak and hole 2.210 (close to iridium atoms) and -2.522 e/ $Å^3$.

Crystal data for **9**: $C_{19}H_{20}BrClIrN$, M_W 569.92, colourless, irregular block (0.155 x 0.142 x 0.107 mm^3), monoclinic, space group $P2_1/c$, *a*: 8.5359(4) Å, *b*: 12.9219(7) Å, *c*: 15.7951(8) Å, *β*: 104.5600(10)°, *V* = 1686.25(15) $Å^3$, *Z* = 4, *Z'* = 1, D_{calc}: 2.245 g cm^{-3}, F(000): 1080, T = 100(2) K, m 10.444 mm^{-1}. 16452 measured reflections (2θ: 3-57°, w scans 0.3°), 4078 unique (R_{int} = 0.0267); min./max. transm. Factors 0.603/0.862. Final agreement factors were R^1 = 0.0199 (3721 observed reflections, I > 2s(I)) and wR^2 = 0.0467; data/restraints/parameters 4078/0/220; GoF = 1.041. Largest peak and hole 1.456 (close to iridium atoms) and -0.668 e/ $Å^3$.

Crystal data for **10**: $C_{29}H_{34}IrNO_4$, M_W 652.77, yellow, irregular block (0.234 x 0.091 x 0.055 mm^3), monoclinic, space group $P2_1/n$, *a*: 9.4133(5) Å, *b*: 20.0386(12) Å, *c*: 13.5666(8) Å, *β*: 94.6470(10)°, *V* = 2550.6(3) $Å^3$, *Z* = 4, *Z'* = 1, D_{calc}: 1.700 g cm^{-3}, F(000):

1296, T = 100(2) K, m 5.270 mm^{-1}. 44848 measured reflections (2θ: 3-57°, w scans 0.3°), 6285 unique (R_{int} = 0.0349); min./max. transm. Factors 0.560/0.862. Final agreement factors were R^1 = 0.0193 (5545 observed reflections, I > 2s(I)) and wR^2 = 0.0439; data/restraints/parameters 6285/0/332; GoF = 1.040. Largest peak and hole 1.052 (close to iridium atoms) and -0.508 e/ $Å^3$.

Crystal data for **11**: $C_{23}H_{26}IrN_3$, 2(BF_4), 1.2(CH_2Cl_2), M_W 812.20, colourless, irregular block (0.168 x 0.120 x 0.100 mm^3), monoclinic, space group C2/c, *a*: 18.7877(10) Å, *b*: 10.7248(6) Å, *c*: 31.060(2) Å, *β*: 103.5140(10)°, *V* = v $Å^3$, *Z* = 8, *Z'* = 1, D_{calc}: 1.773 g cm^{-3}, F(000): 3155, T = 100(2) K, m 4.668 mm^{-1}. 42894 measured reflections (2θ: 3-57°, w scans 0.3°), 7401 unique (R_{int} = 0.0526); min./max. transm. Factors 0.713/0.862. Final agreement factors were R^1 = 0.0441 (5917 observed reflections, I > 2s(I)) and wR^2 = 0.1165; data/restraints/parameters 7401/29/366; GoF = 1.038. Largest peak and hole 1.944 (close to iridium atoms) and -1.838 e/ $Å^3$.

Crystal data for **12**: $C_{24}H_{27}IrNO_2$, BF_4, 0.5($C_4H_{10}O$), M_W 677.53, brown, irregular block (0.126 x 0.124 x 0.100 mm^3), hexagonal, space group P6/5, *a*: 10.9926(6) Å, *b*: 10.9926(6) Å, *c*: 72.259(4) Å, *V* = 7561.7(9) $Å^3$, *Z* = 12, *Z'* = 2, D_{calc}: 1.785 g cm^{-3}, F(000): 3996, T = 100(2) K, m 5.353 mm^{-1}. 136315 measured reflections (2θ: 3-57°, w scans 0.3°), 12694 unique (R_{int} = 0.1186); min./max. transm. Factors 0.687/0.862. Final agreement factors were R^1 = 0.0507 (10006 observed reflections, I > 2s(I)) and wR^2 = 0.0824; data/restraints/parameters 12694/45/646; GoF = 1.073. Largest peak and hole 0.850 (close to iridium atoms) and -0.952 e/ $Å^3$.

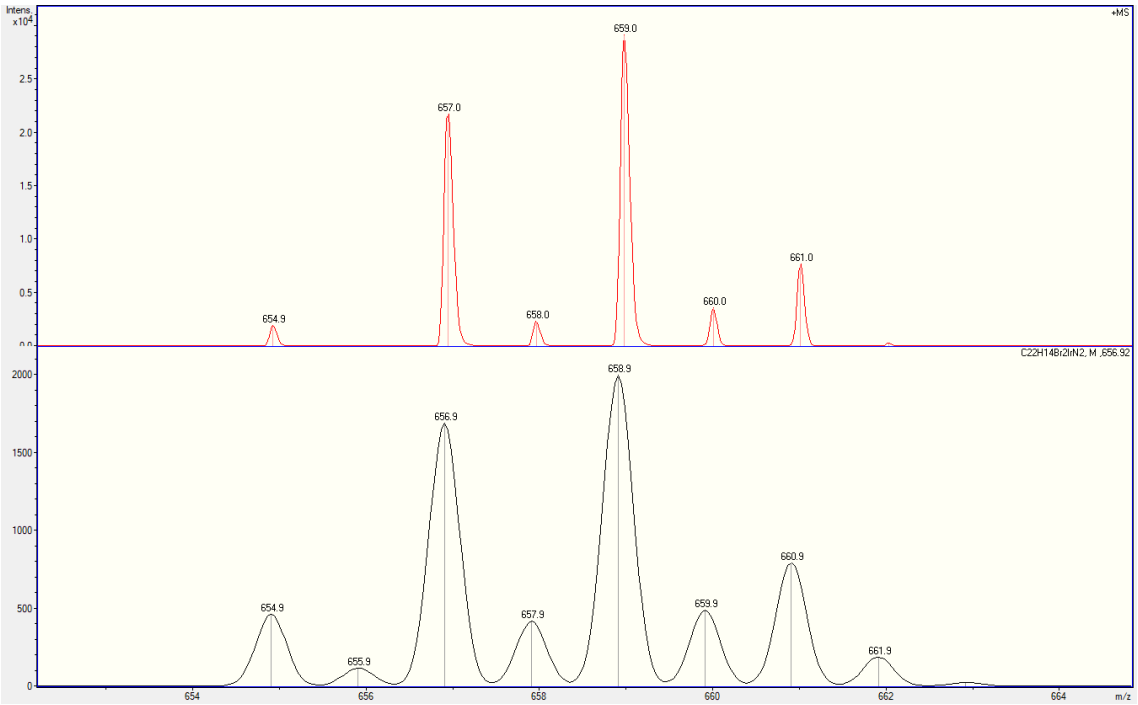

Figure S4. MALDI-TOF of complex $(\eta^2\text{-}C_8H_{14})_2Ir(\mu\text{-}Cl)_2Ir\{\kappa^2\text{-}C,N\text{-}[C_6BrH_3\text{-}py]\}_2$ **(3).**

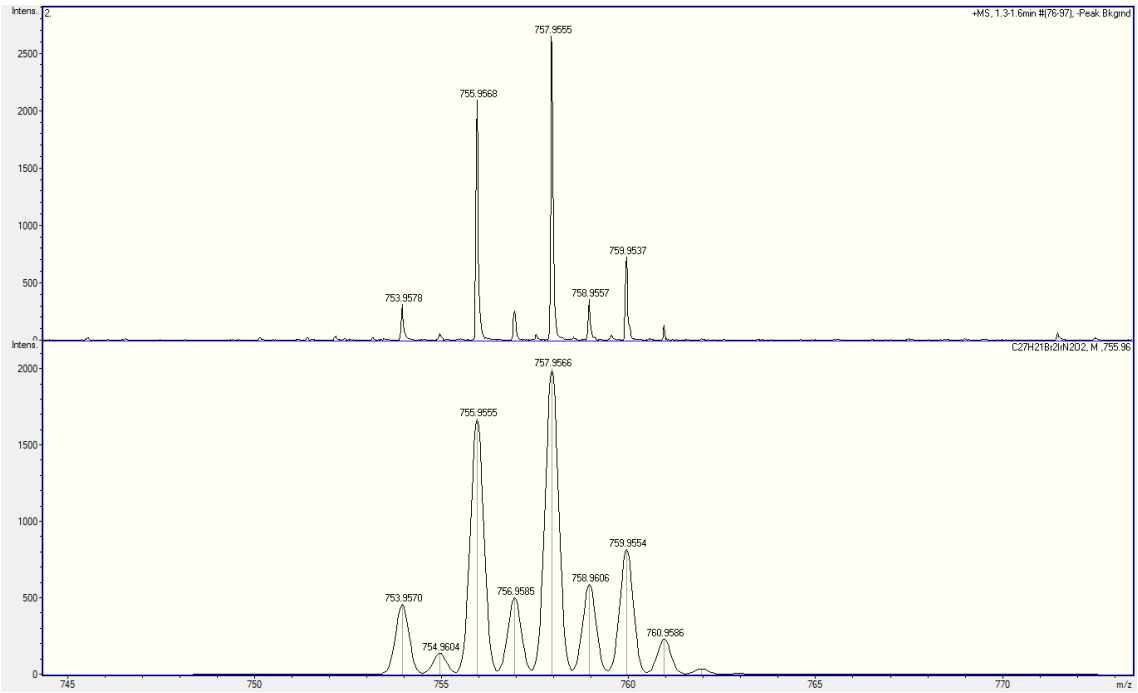

Figure S5. MALDI-TOF of complex $Ir(acac)\{\kappa^2\text{-}C,N\text{-}[C_6BrH_3\text{-}py]\}_2$ (**5**)

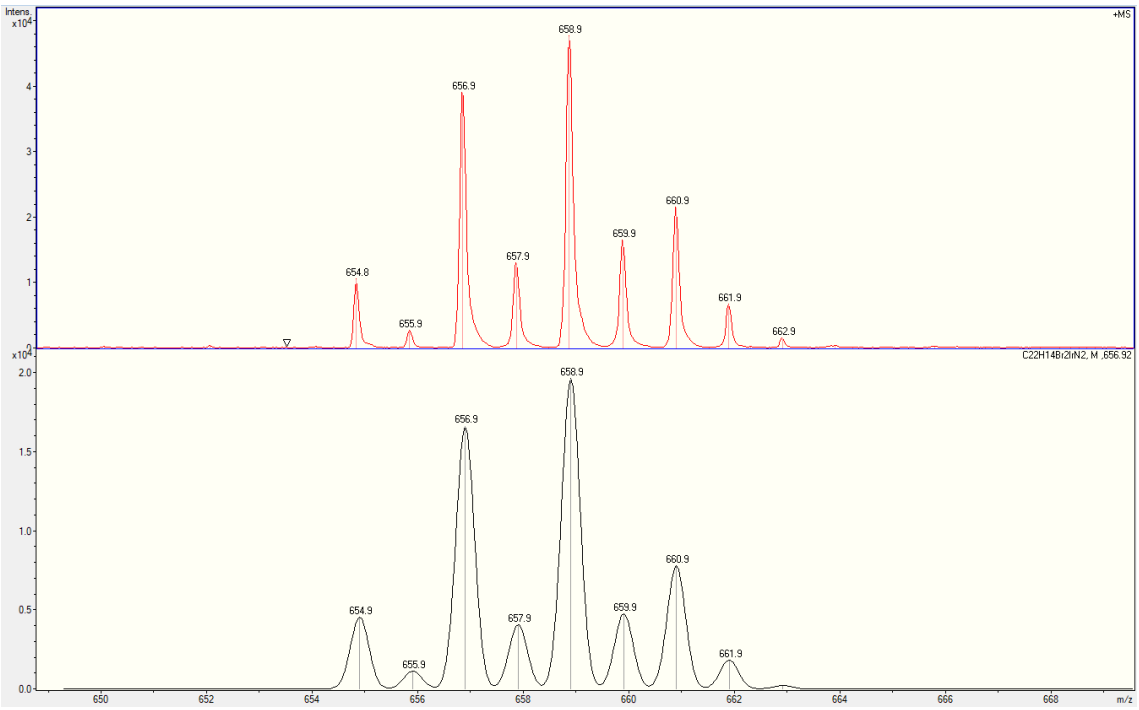

Figure S6. MALDI-TOF of Ir{κ^2-*C,N*-[C_6BrH_3-py]}$_2$ fragment.

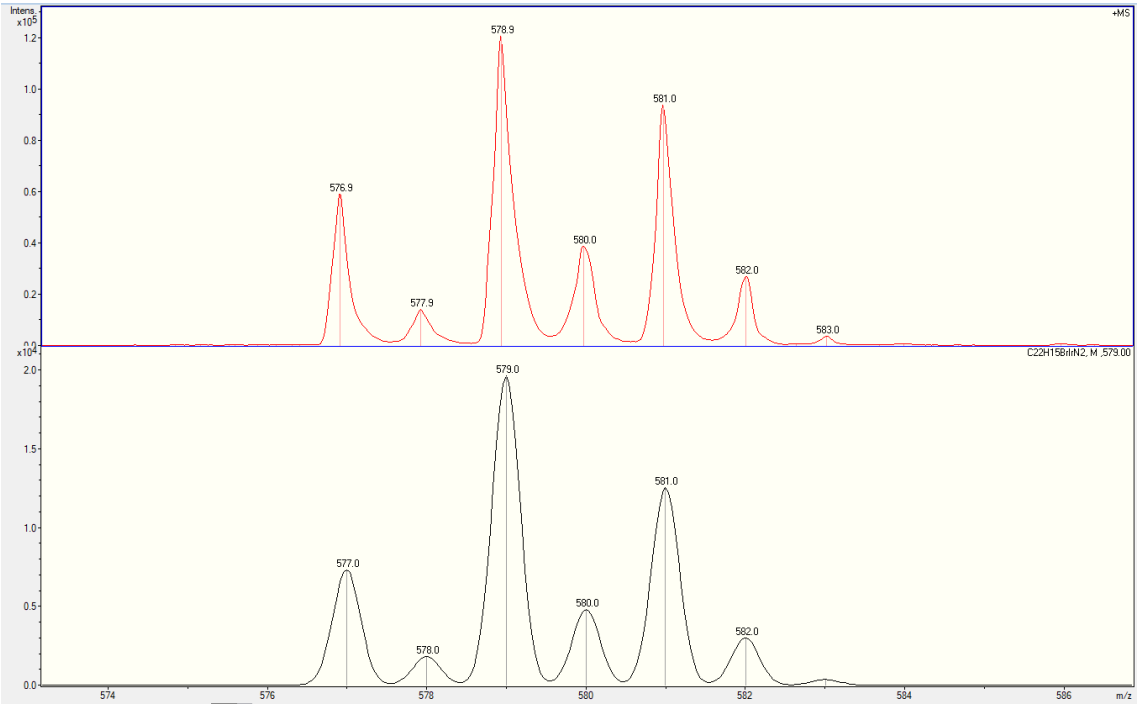

Figure S7. MALDI-TOF of Ir{κ^2-*C,N*-[C_6BrH_3-py]} {κ^2-*C,N*-[C_6H_4-py]}fragment.

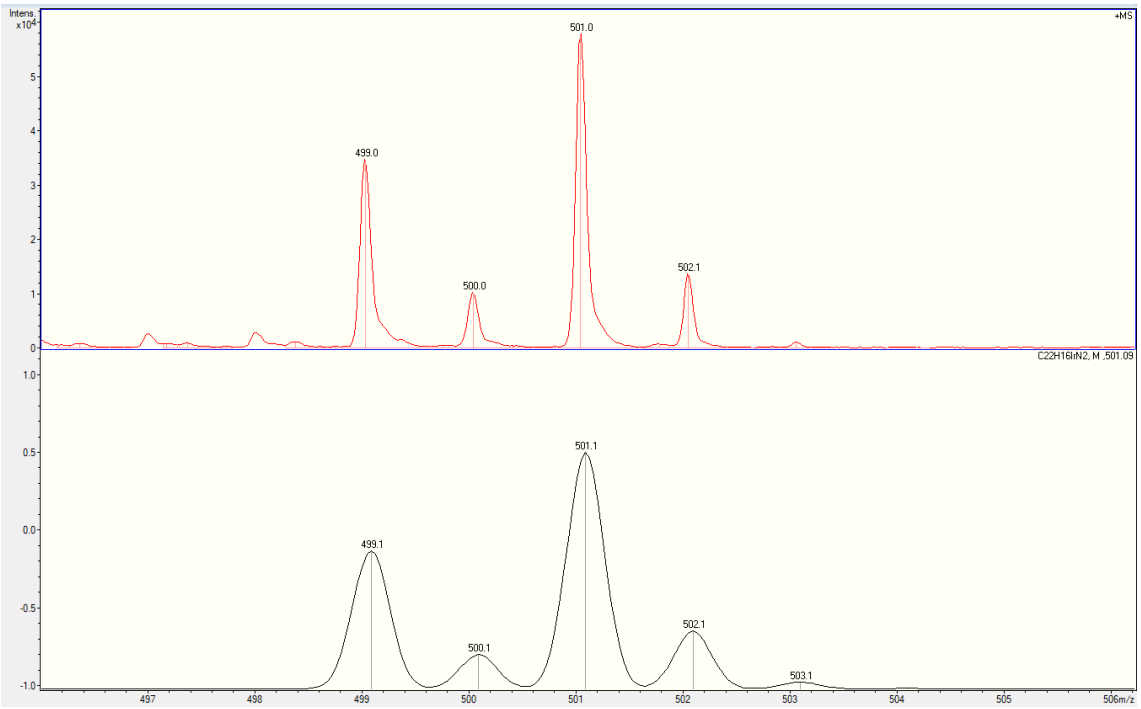

Figure S8. MALDI-TOF of Ir{κ^2-*C,N*-[C_6H_4-py]}$_2$ fragment.

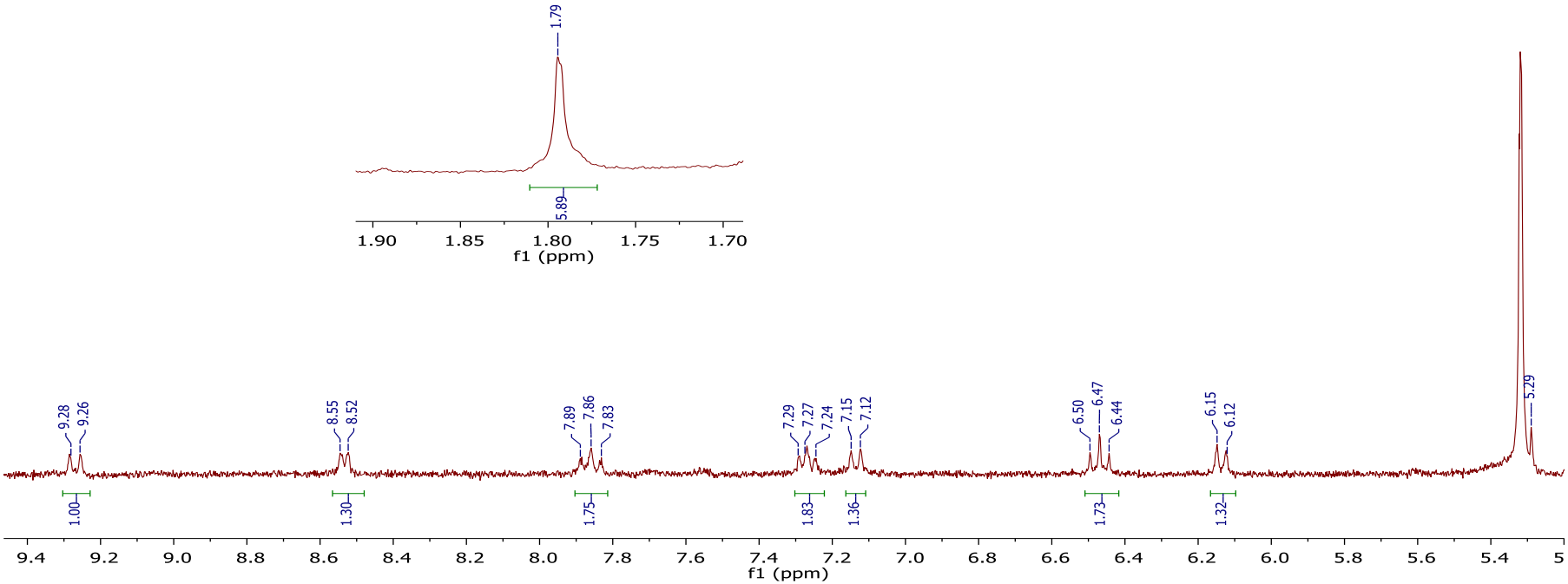

Figure S9. ^{1}H-NMR (300 MHz, CD_2Cl_2, 298 K) spectra of Ir(acac){κ^2-*C,N*-[C_6BrH_3-py]}$_2$ (**5**)

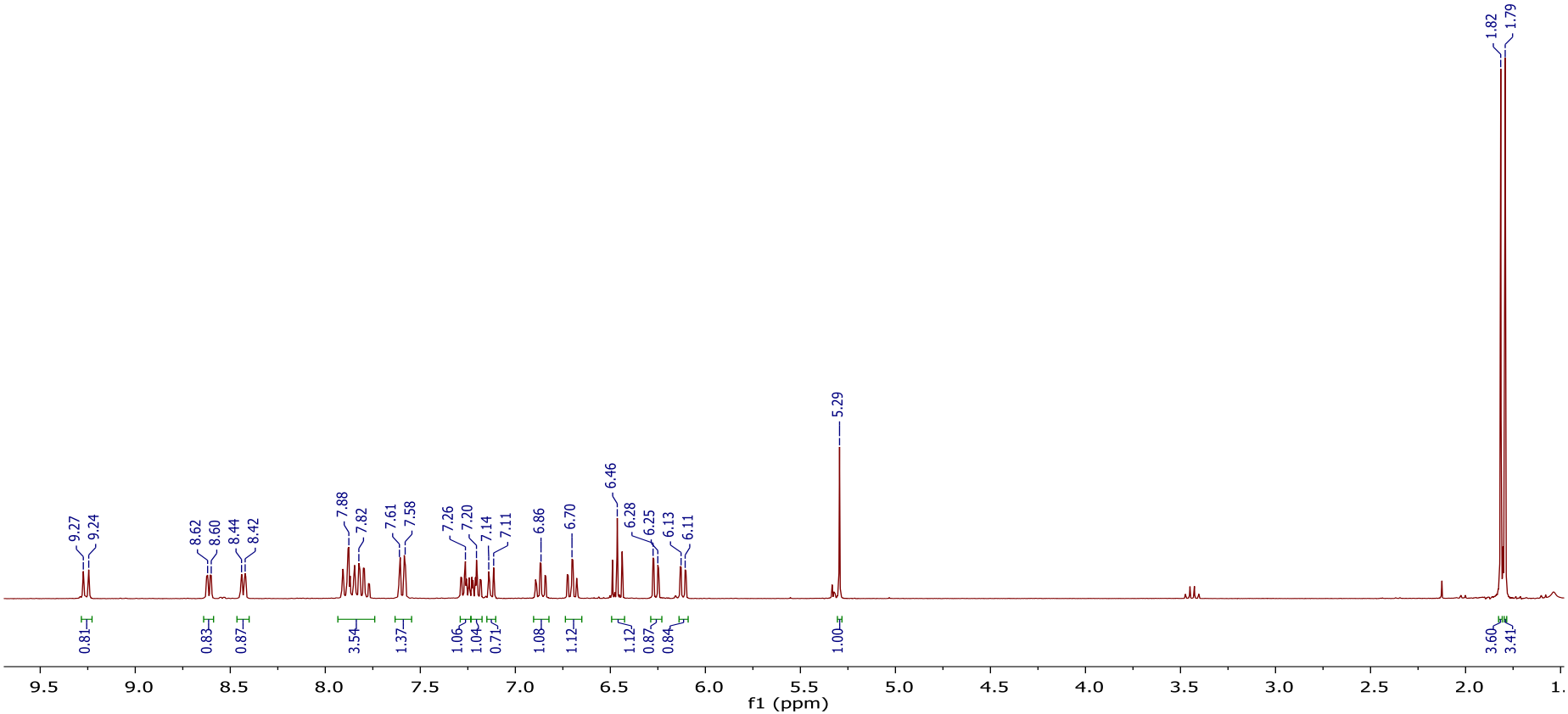

Figure S10. ^{1}H-NMR (300 MHz, CD_2Cl_2, 298 K) of Ir(acac){κ^2-*C,N*-[C_6BrH_3-py]}{κ^2-*C,N*-[C_6H_4-py]} (**6**)

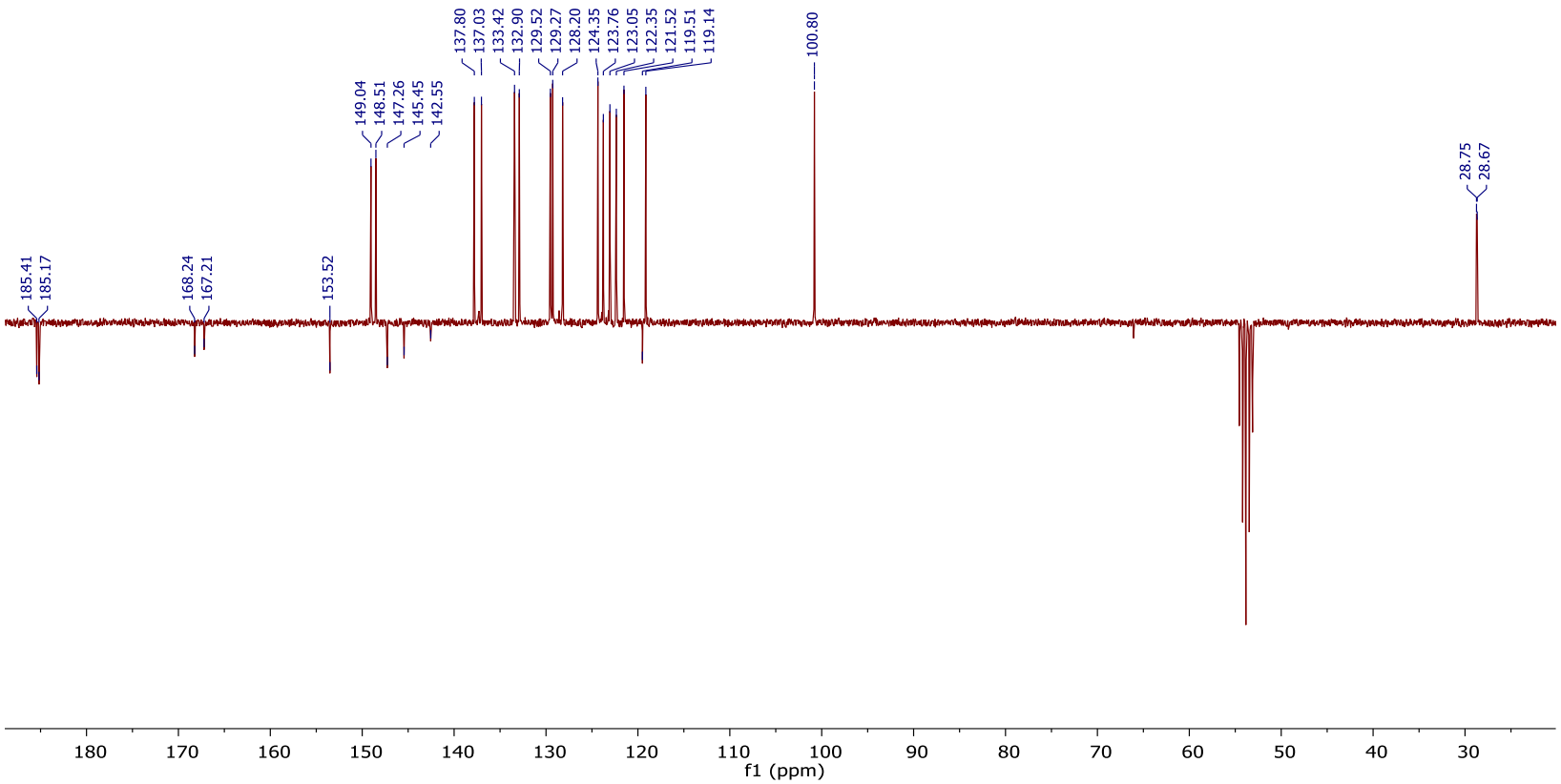

Figure S11. $^{13}C\{^{1}H\}$ APT NMR (75 MHz, CD_2Cl_2, 298 K) of Ir(acac){κ^2-*C,N*-[C_6BrH_3-py]}{κ^2-*C,N*-[C_6H_4-py]} (**6**)

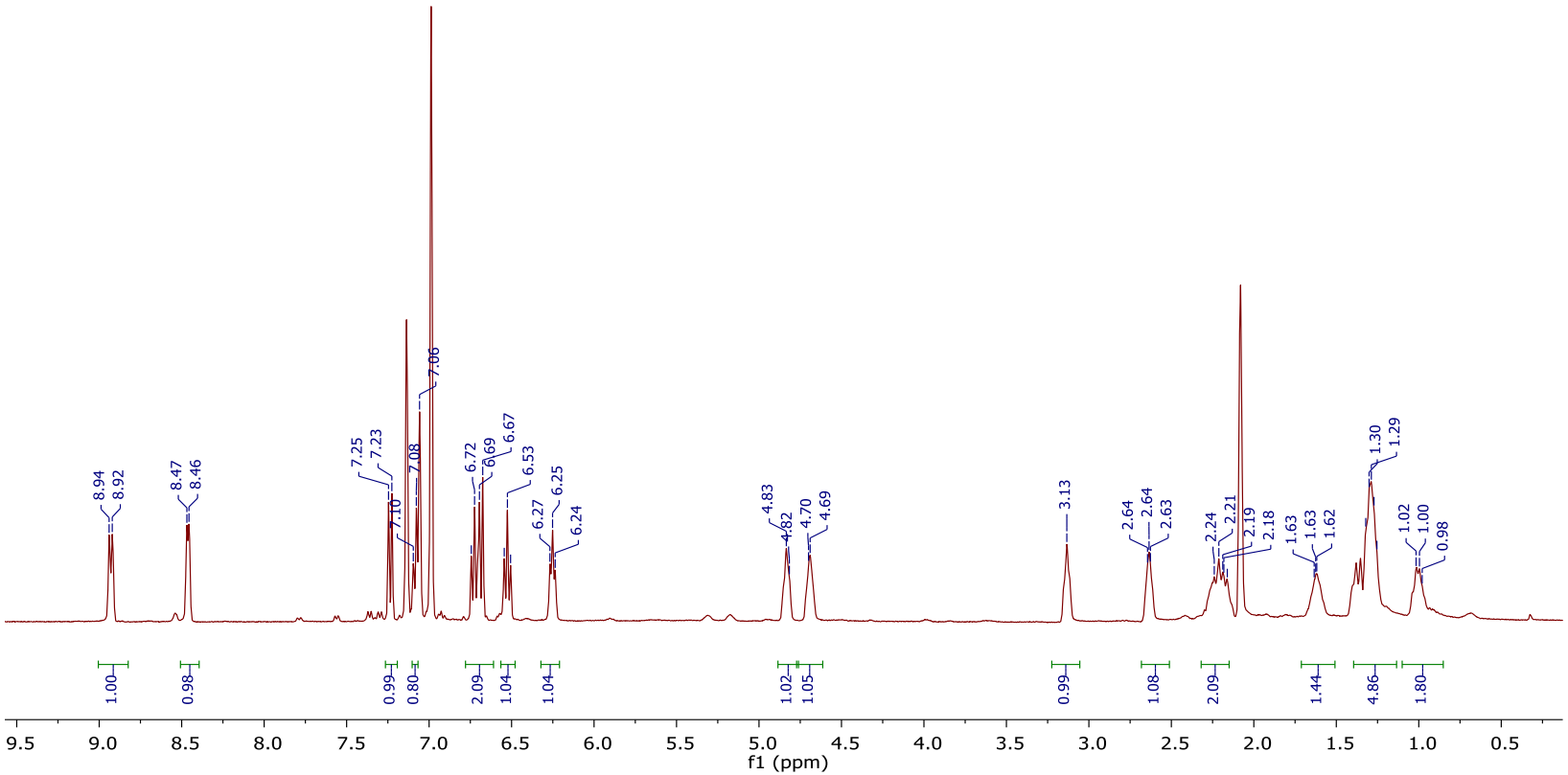

Figure S12. ^{1}H-NMR (400 MHz, tol-d_8, 223K) for IrCl(η^4-C_8H_{12}){κ^1-*N*-[py-C_6BrH]}(**8**).

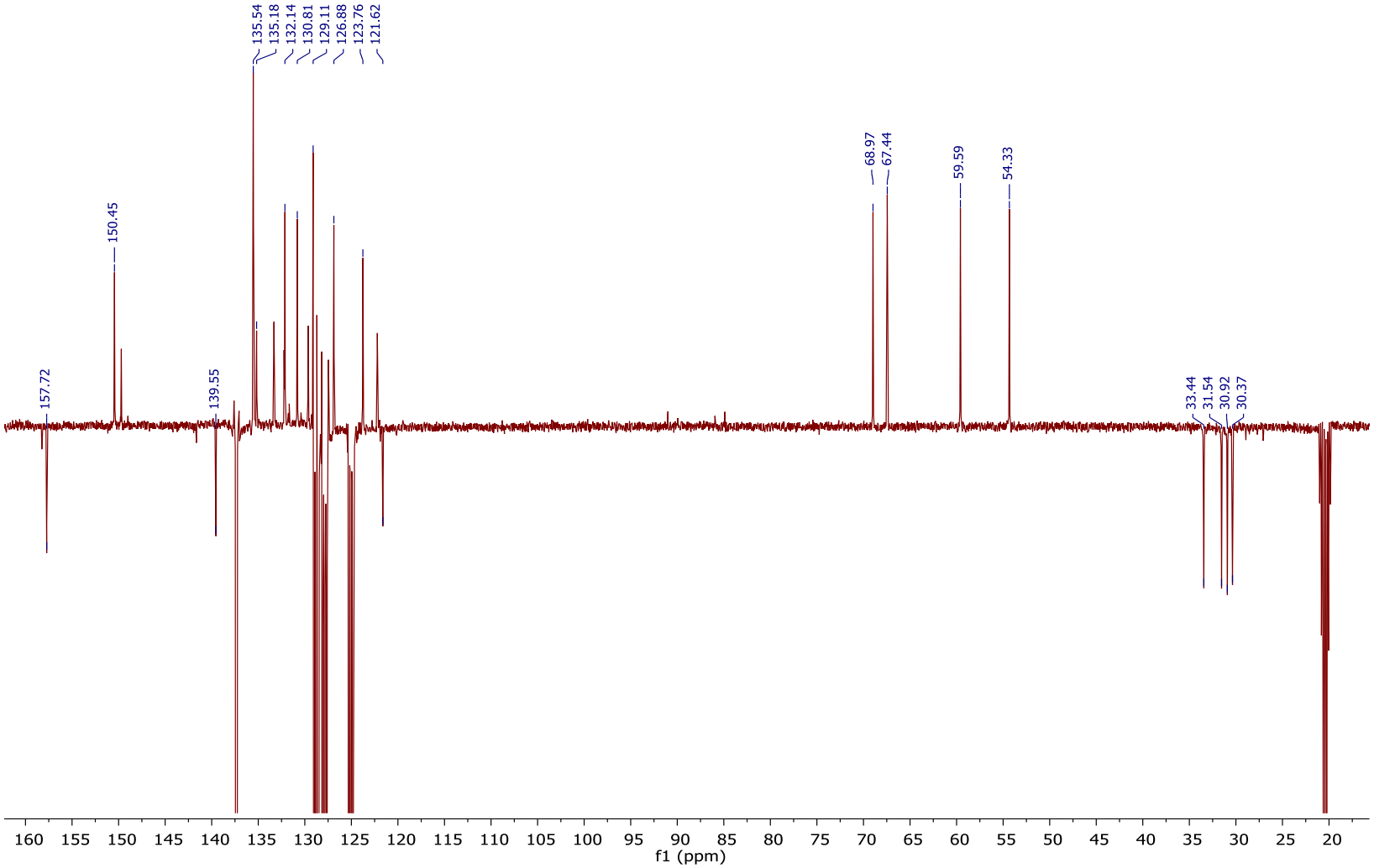

Figure S13. $^{13}C\{^{1}H\}$ APT NMR (100 MHz, tol-d_8, 223K) for IrCl(η^4-C_8H_{12}){κ^1-*N*-[py-C_6BrH]}(**8**).

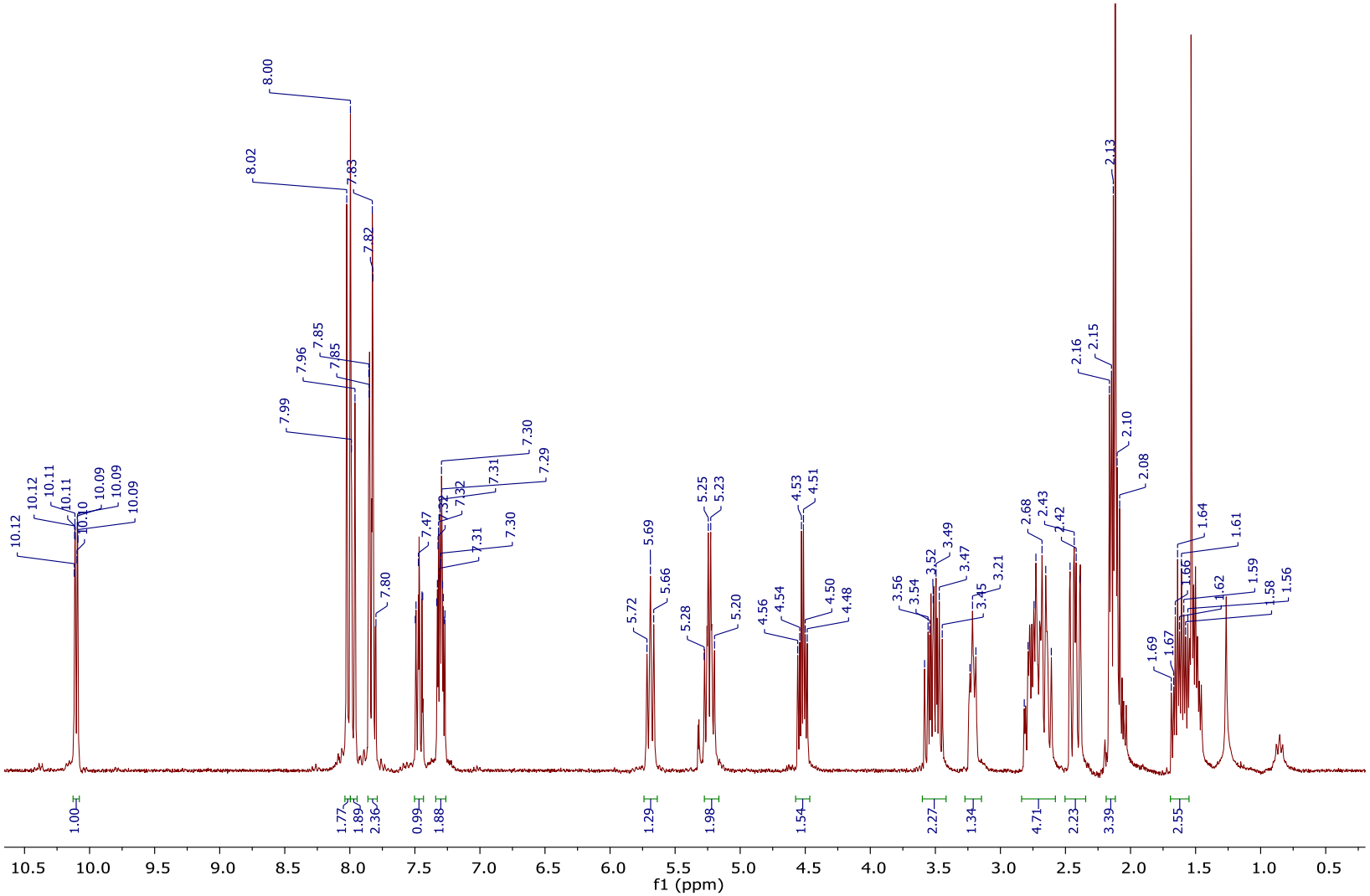

Figure S14. ^{1}H-NMR (300 MHz, CD_2Cl_2, 298 K) of IrClBr{κ^2-*C,N*-[C_6H_4-py]}(η^4-C_8H_{12}) (**9**).

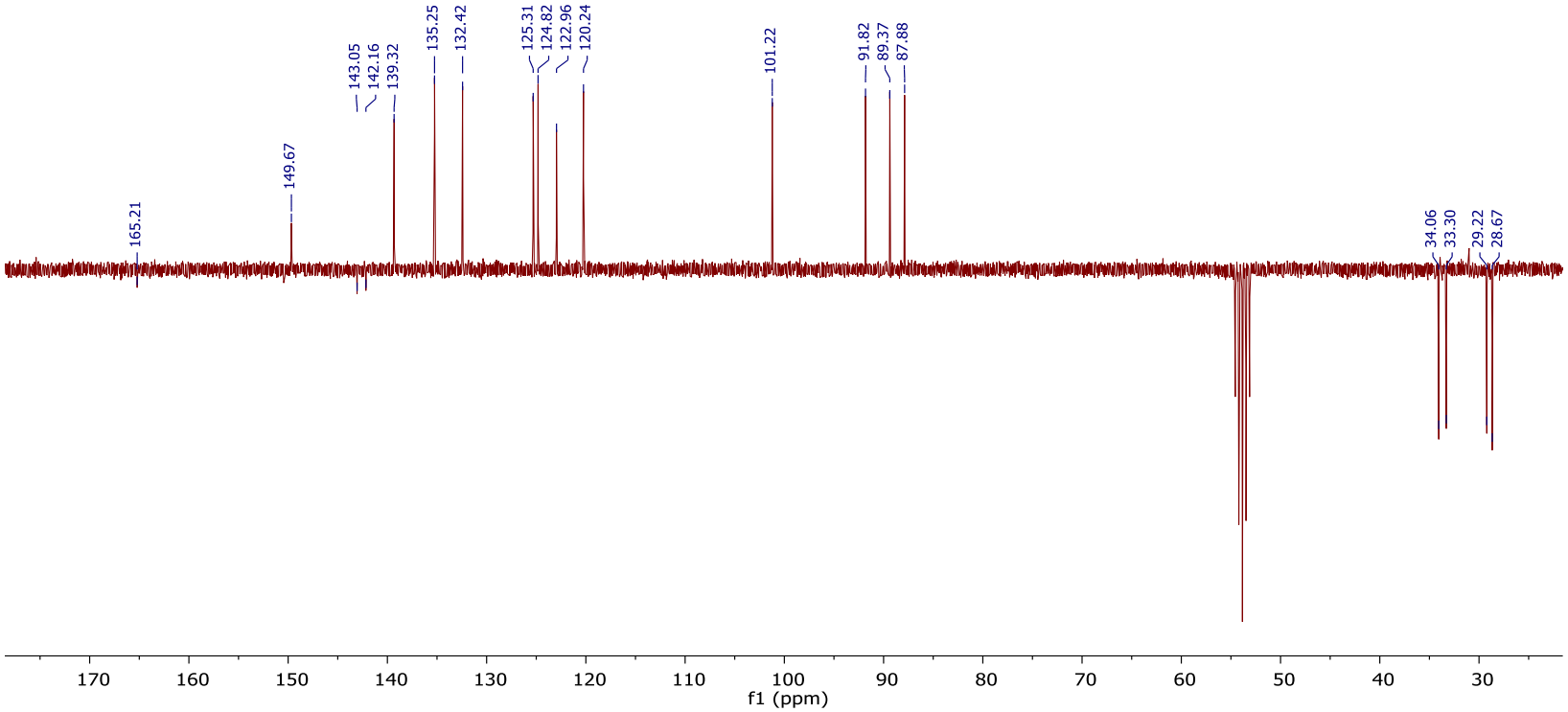

Figure S15. $^{13}C\{^{1}H\}$ APT NMR (75 MHz, CD_2Cl_2, 298 K) for IrClBr{κ^2-*C,N*-[C_6H_4-py]}(η^4-C_8H_{12}) (**9**).

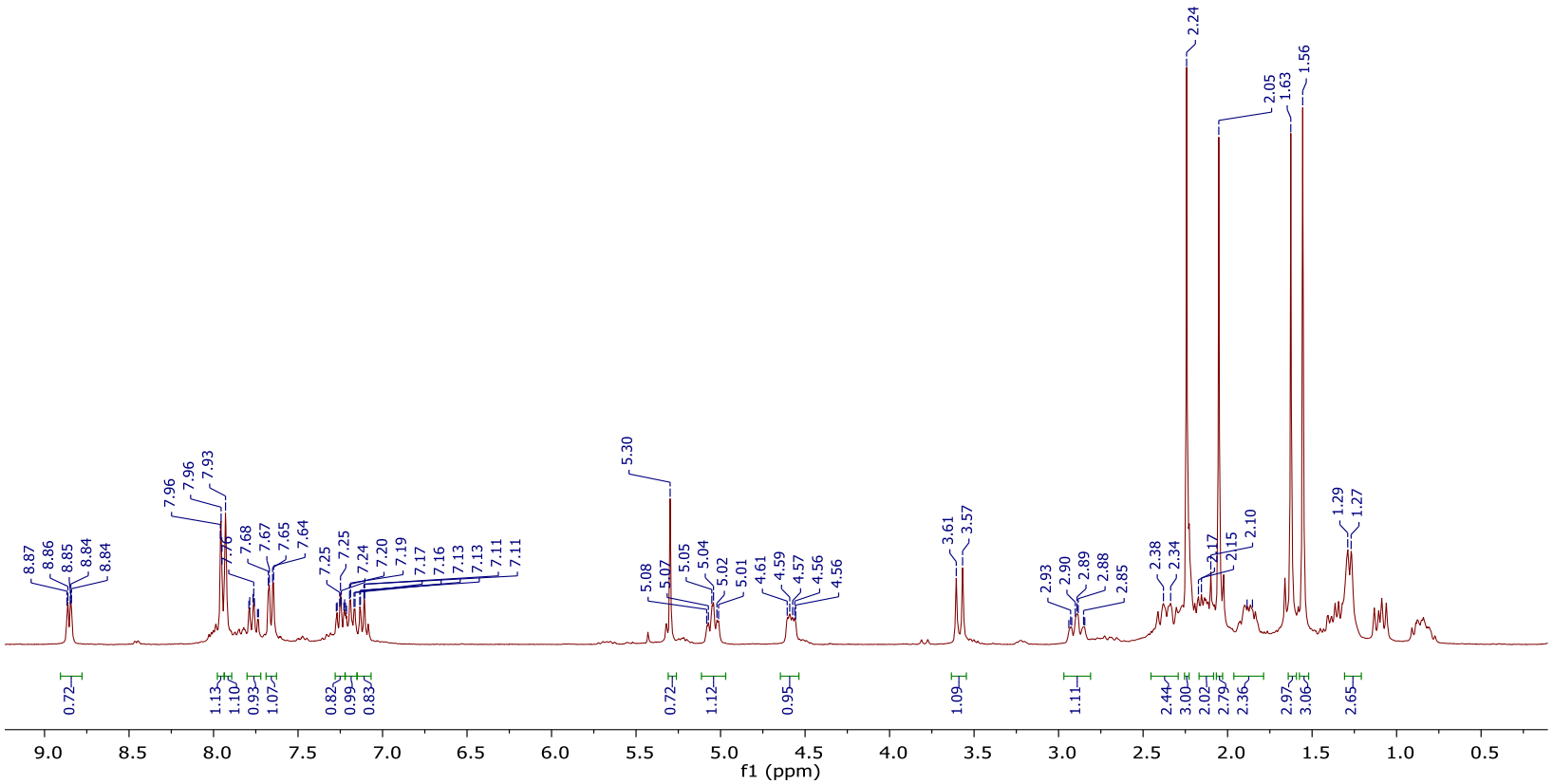

Figure S16. ^{1}H-NMR (300 MHz, CD_2Cl_2, 298 K) for Ir(acac){κ^2-*C,N*-[C_6H_4-py]}{κ^1-*C*, η^2-[C_8H_{12}-(C^3-acac)]} (**10**)

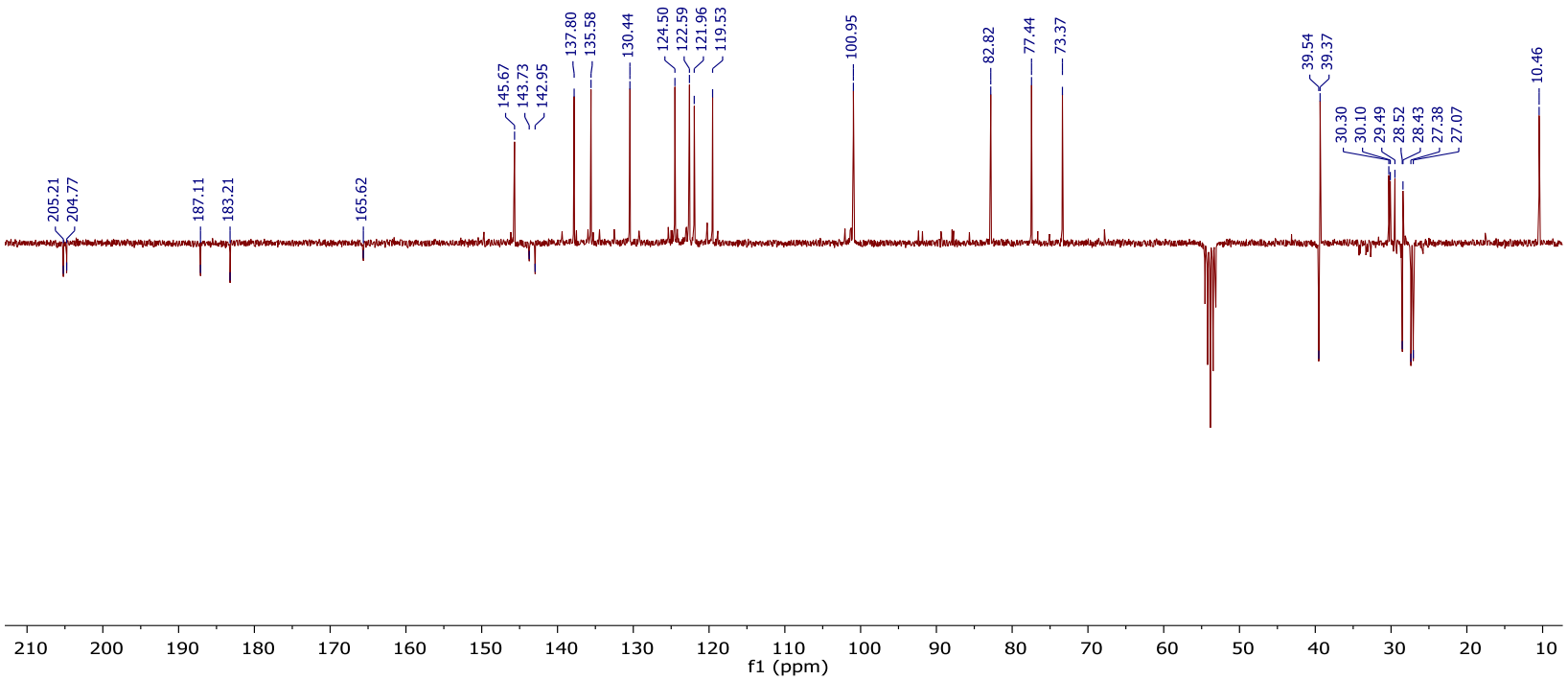

Figure S17. $^{13}C\{^{1}H\}$ APT NMR (75 MHz, CD_2Cl_2, 298 K) for Ir(acac){κ^2-*C,N*-[C_6H_4-py]}{κ^1-*C*, η^2-[C_8H_{12}-(C^3-acac)]} (**10**).

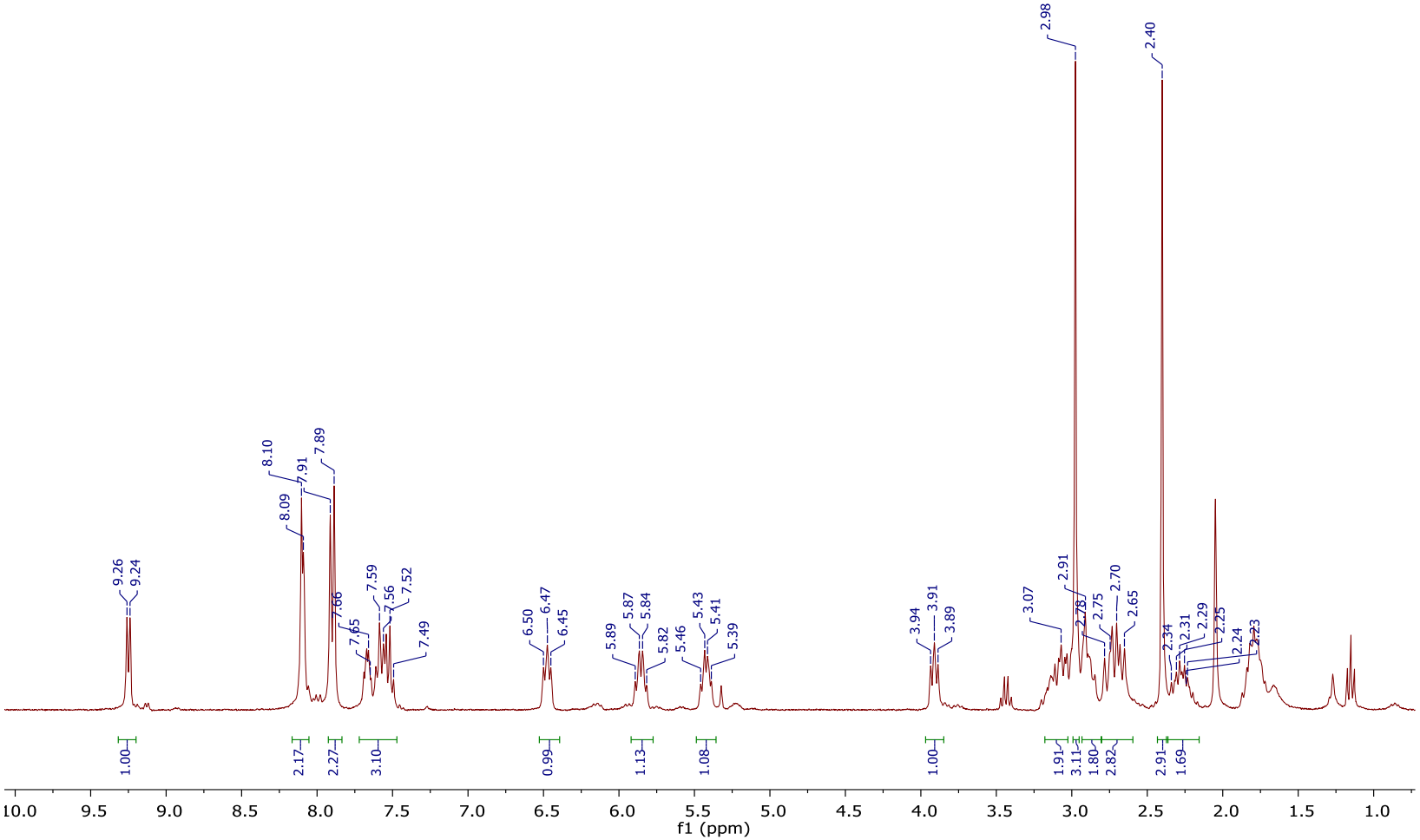

Figure S18. ^{1}H-NMR (300 MHz, CD_2Cl_2, 298 K) for [Ir{κ^2-*C,N*-[C_6H_4-py]}(η^4-C_8H_{12})(CH_3CN)$_2$](BF_4)$_2$ (**11**)

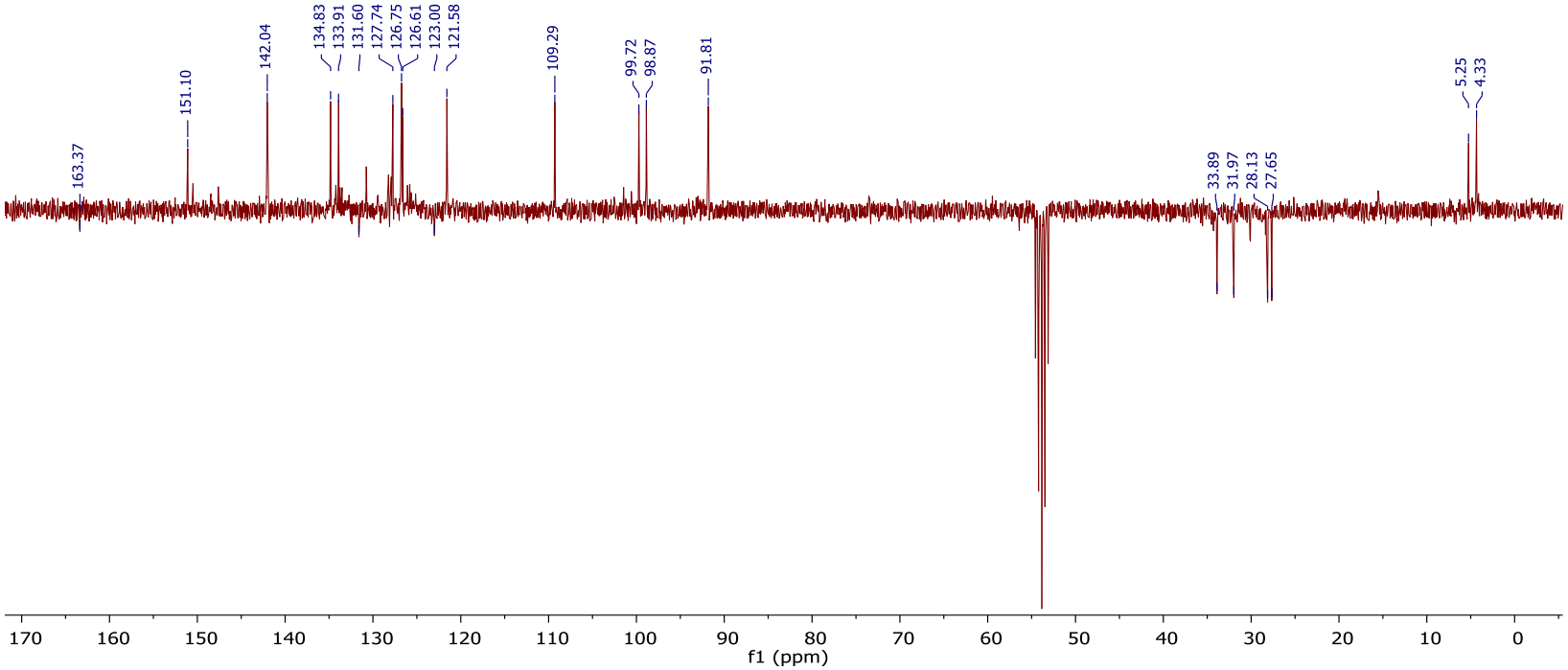

Figure S19. $^{13}C\{^{1}H\}$ APT NMR (75 MHz, CD_2Cl_2, 298 K) for $[Ir\{\kappa^2\text{-}C,N\text{-}[C_6H_4\text{-py}]\}(\eta^4\text{-}C_8H_{12})(CH_3CN)_2](BF_4)_2$ (**11**)

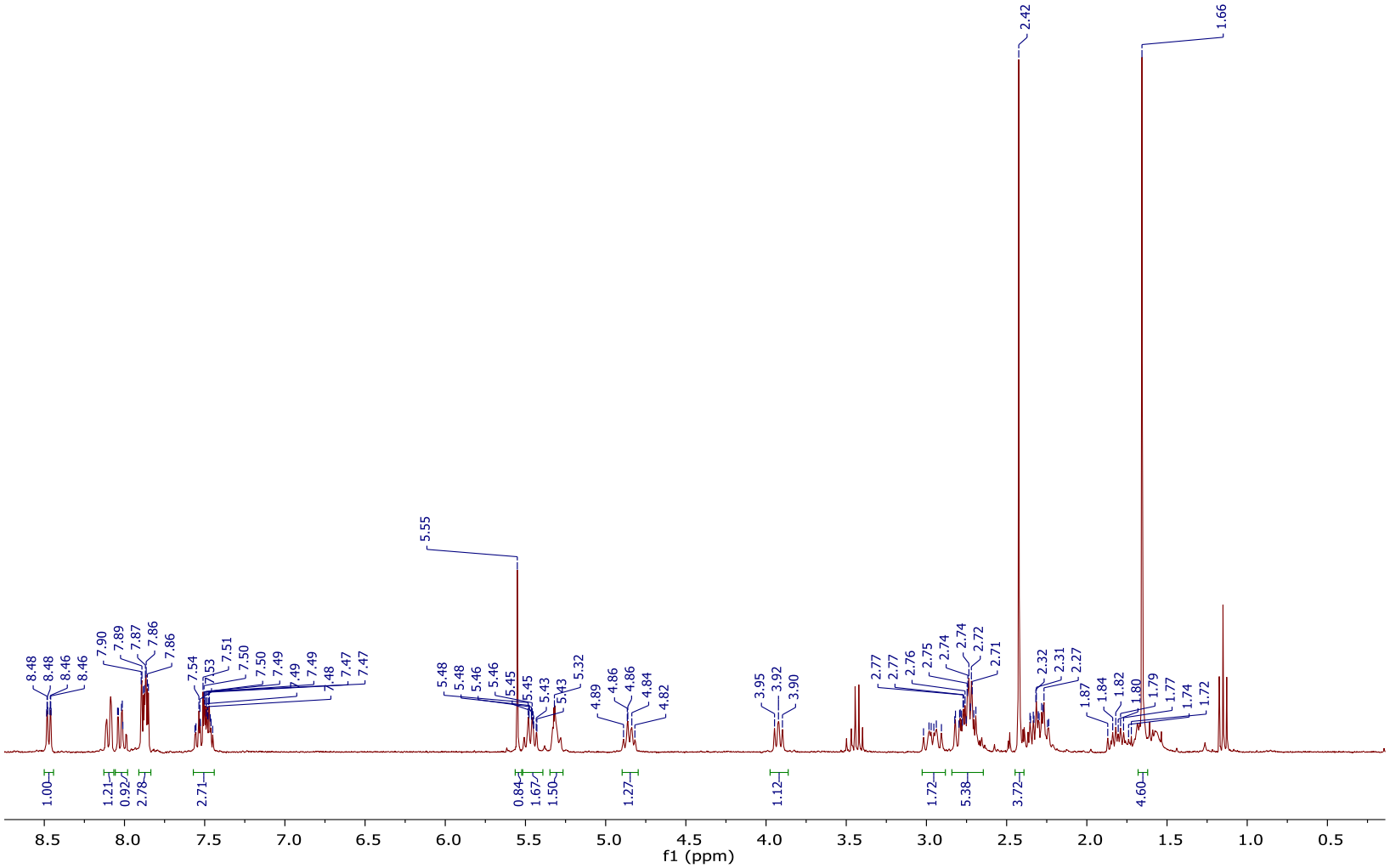

Figure S20. ^{1}H-NMR (300 MHz, CD_2Cl_2, 298 K) for [Ir(acac){κ^2-*C,N*-[C_6H_4-py]}(η^4-C_8H_{12})]BF_4 (**12**).

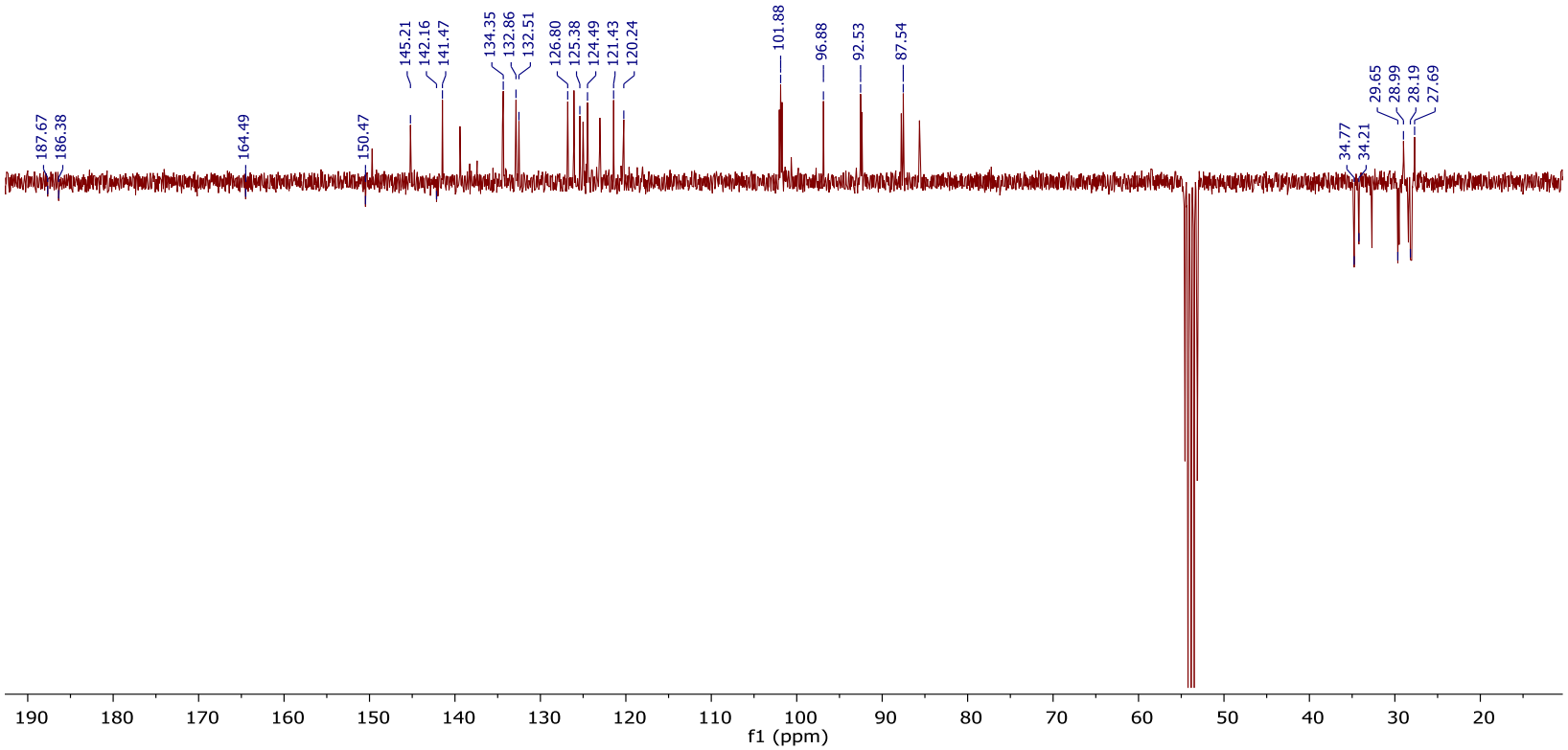

Figure S21. $^{13}C\{^{1}H\}$ APT NMR (75 MHz, CD_2Cl_2, 298 K) for [Ir(acac){κ^2-*C,N*-[C_6H_4-py]}(η^4-C_8H_{12})]BF_4 (**12**).

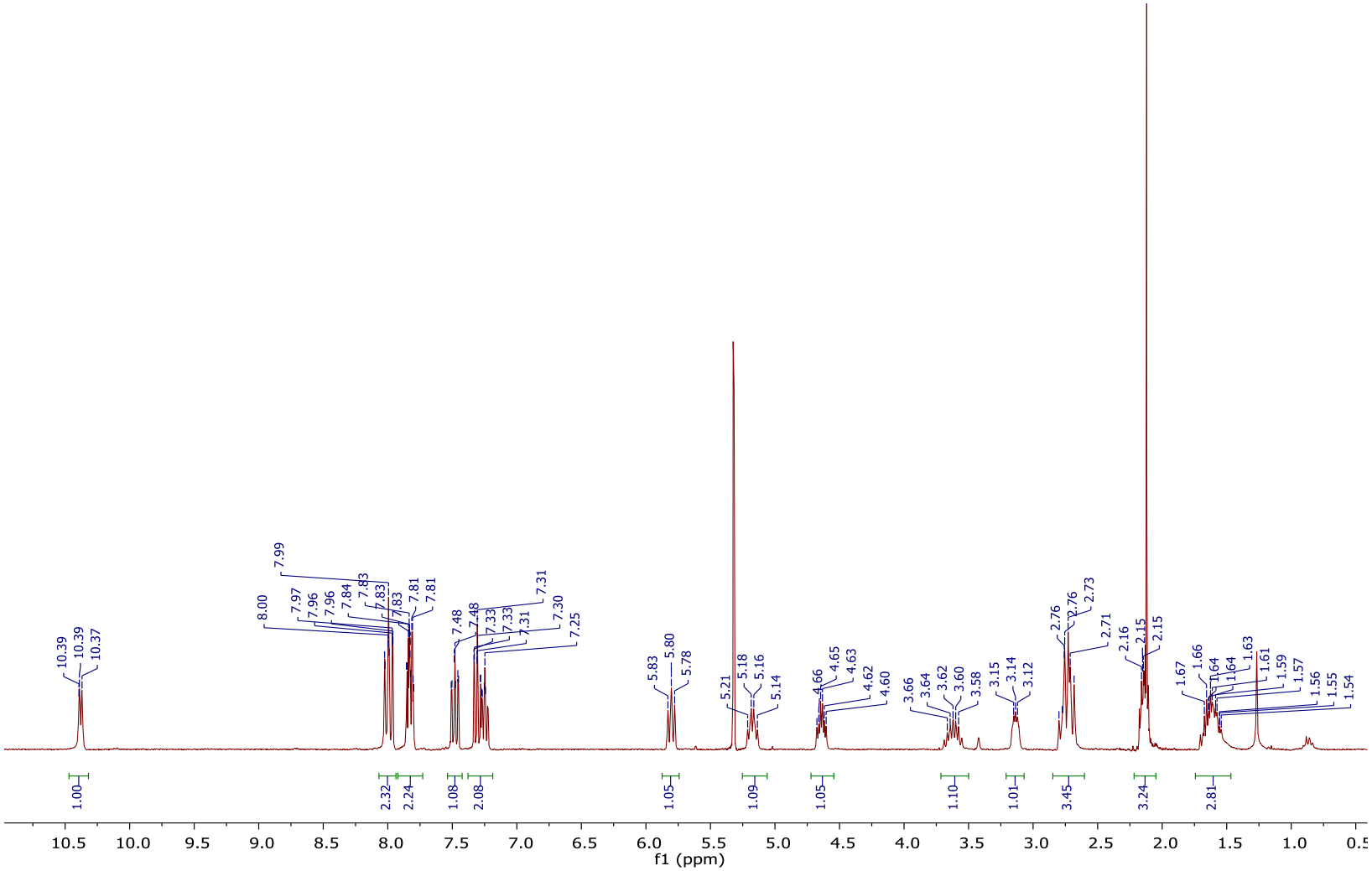

Figure S22. ^{1}H-NMR (300 MHz, CD_2Cl_2, 298 K) for $IrBr_2\{\kappa^2\text{-}C,N\text{-}[C_6H_4\text{-py}]\}(\eta^4\text{-}C_8H_{12})$ (**13**).

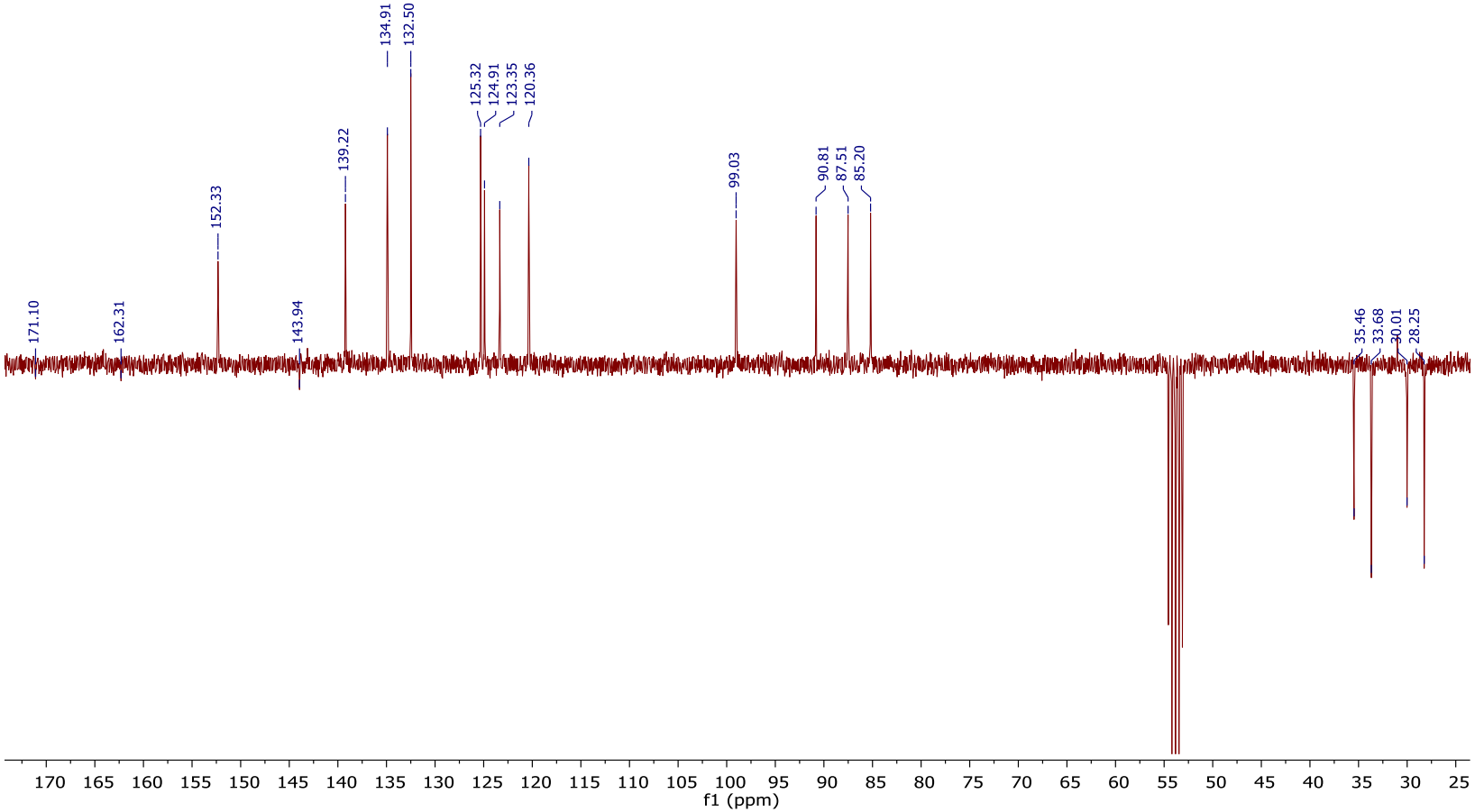

Figure S23. $^{13}C\{^{1}H\}$ APT NMR (75 MHz, CD_2Cl_2, 298 K) for $IrBr_2\{\kappa^2\text{-}C,N\text{-}[C_6H_4\text{-py}]\}(\eta^4\text{-}C_8H_{12})$ (**13**).

REFERENCES

(1) Blessing, R. H. *Acta Crystallogr.* **1995**, *A51*, 33. SADABS: Area-detector absorption correction; Bruker- AXS, Madison, WI, 1996.

(2) SHELXL-2016/6. Sheldrick, G. M. *Acta Cryst.* **2008**, *A64*, 112-122.